RESEARCH PAPER

Relating surface-enhanced Raman scattering signals of cells to gold nanoparticle aggregation as determined by LA-ICP-MS micromapping

Tina Büchner · Daniela Drescher · Heike Traub ·
Petra Schrade · Sebastian Bachmann ·
Norbert Jakubowski · Janina Kneipp

Abstract The cellular response to nanoparticle exposure is essential in various contexts, especially in nanotoxicity and nanomedicine. Here, 14-nm gold nanoparticles in 3T3 fibroblast cells are investigated in a series of pulse-chase experiments with a 30-min incubation pulse and chase times ranging from 15 min to 48 h. The gold nanoparticles and their aggregates are quantified inside the cellular ultrastructure by laser ablation inductively coupled plasma mass spectrometry micromapping and evaluated regarding the surface-enhanced Raman scattering (SERS) signals. In this way, both information about their localization at the micrometre scale and their molecular nanoenvironment, respectively, is obtained and can be related. Thus, the nanoparticle pathway from endocytotic uptake, intracellular processing, to cell division can be followed. It is shown that the ability of the intracellular nanoparticles and their accumulations and aggregates to support high SERS signals is neither directly related to nanoparticle amount nor to high local nanoparticle densities. The SERS data indicate that aggregate geometry and interparticle distances in the cell must change in the course of endosomal maturation and play a critical role for a specific gold nanoparticle type in order to act as efficient SERS nanoprobe. This finding is supported by TEM images, showing only a minor portion of aggregates that present small interparticle spacing. The SERS spectra obtained after different chase times show a changing composition and/or structure of the biomolecule corona of the gold nanoparticles as a consequence of endosomal processing.

T. Büchner · D. Drescher · J. Kneipp (✉)
Department of Chemistry, Humboldt-Universität zu Berlin,
Brook-Taylor-Str. 2, 12489 Berlin, Germany
e-mail: janina.kneipp@chemie.hu-berlin.de

T. Büchner · D. Drescher · H. Traub · N. Jakubowski · J. Kneipp
BAM Federal Institute for Materials Research and Testing,
Richard-Willstätter-Str. 11, 12489 Berlin, Germany

P. Schrade · S. Bachmann
Department of Anatomy, Charité Universitätsmedizin, Charitéplatz
1, 10117 Berlin, Germany

Introduction

Due to their unique physical and chemical properties, gold nanoparticles are widely used for analytical approaches [1, 2], in molecular plasmonics [3, 4], and nanomedicine [5–8]. In order to evaluate nano-bio-interactions, which are, e.g., relevant in elucidating nanoparticle toxicity, the interactions of the nanoparticles with cellular molecules, their localization in the cellular ultrastructure, and their quantity inside cells or living organisms must be known. As we have shown previously, a combination of different analytical and imaging approaches giving qualitative, quantitative, and ultrastructural information is necessary to understand the different aspects of nanoparticle–cell interactions [9, 10]. Merging this information for a biological interpretation clearly poses a current challenge, and care has to be taken in evaluating the role of a particular method in the elucidation of a certain aspect. For example, as revealed by combining information from nanotomography with vibrational spectroscopy, the intracellular localization and nanoparticle aggregate morphology are strongly

influenced by the molecules adsorbed to the nanoparticle surface [9].

In the case of gold nanoparticles, the local fields generated upon excitation of their localized surface plasmons enable sensitive probing of the molecules interacting with the particle surface on the nanometer scale within living cells by surface-enhanced Raman scattering (SERS) [11–13]. SERS can also be used for sensing of general chemical parameters in the cellular nanoenvironment, such as progressing acidification in endosomes [14, 15] using nanoprobes containing a pH-sensitive reporter molecule [12, 16, 17].

The quantification of nanoaggregates in cells is of particular importance to obtain information on particle uptake and distribution under different experimental conditions. Optical methods, specifically SERS imaging [13, 18] or dark field microscopy [19–21] rely on plasmonic properties, which alter under the incubation conditions and during cellular uptake with the formation of nanoparticle aggregates. Both the amount of nanoparticles but also the processing inside the cells may have an influence on aggregate formation. With respect to SERS enhancement, which is strongest in hot spots formed in nanoparticle aggregates, the geometry of the aggregates, specifically the arrangement of individual nanoparticles [22], and the gap size between them [23, 24] are a crucial determinant. Inside the cell, nanoparticle aggregate morphology is governed by the interaction with cellular molecules and the behavior of vesicular substructures, which will depend on the size and surface properties of the nanoparticles [9, 13]. Therefore, the suitability of one particular type of plasmonic nanoparticle to act as intracellular nanoprobe can vary greatly from that of another one.

The number of inorganic nanoparticles is often determined by elemental analysis using atomic absorption spectrometry, inductively coupled plasma (ICP) optical emission spectrometry or inductively coupled plasma mass spectrometry (ICP-MS) after acid digestion of a cell suspension or pellet [25, 26] with the disadvantage that no spatial information on the particle distribution and potential formation of nanoparticle accumulations within an individual cell is available. For elemental mapping of biological samples such as tissues or cells [27–30], laser ablation inductively coupled plasma mass spectrometry (LA-ICP-MS) has proven to be a powerful analytical tool, offering excellent sensitivity at high spatial resolution and multielement capability. In previous studies, we have shown that quantification of metal nanoparticles can be achieved at the single-cell level by LA-ICP-MS and that the capabilities of this approach can be extended to spatially resolved LA-ICP-MS micromapping [31, 10].

Here, we apply the ability to quantify gold nanoparticles by LA-ICP-MS micromapping to study smaller gold nanoparticles of ~14 nm diameter and their accumulation and distribution in 3T3 fibroblast cells during cellular uptake, processing, and mitosis. Pulse-chase experiments with different chase times were conducted to follow the particle processing in vivo. We obtain information on the local gold concentration that comprises accumulation of gold nanoparticles in endosomal structures and formation of aggregates at different time points during endosomal maturation. The influence of aggregate geometry and interparticle distance is very sensitive to the cellular environment, where the inclusion of the nanostructures in vesicles of partly complicated ultrastructure can lead to drastic changes in the size of interparticle gaps. By SERS, qualitative information is obtained on the molecules and molecular groups that are in the immediate environment of the nanostructures and at their surface. Moreover, as the SERS enhancement factors obtained with individual nanoparticles are relatively low, the influence of nanoaggregate formation, and aggregate geometry, on the SERS enhancement is reflected in both the overall intensities and in the number of SERS spectra that can be obtained from a cell. By combining the information about the number of spots in a cell containing nanoaggregates (from LA-ICP-MS) with the number of probed volumes yielding SERS signals, we obtain information on the portion of nanoaggregates that provide suitable plasmonic properties at a specific time point during nanomaterial processing. This information is useful in order to evaluate the intracellular applicability of specific nanoparticles as SERS probes, e.g., in biotechnological applications.

Materials and methods

Nanoparticle synthesis and characterization

For the preparation of gold nanoparticles gold(III)chloride trihydrate (99.9 %, Sigma-Aldrich, Taufkirchen, Germany) and trisodium citrate dihydrate (99 %, Merck, Darmstadt, Germany) were purchased. According to [32], 250 mL of 1 mM gold(III)chloride trihydrate solution was boiled for 10 min before 25 mL of 40 mM trisodium citrate dehydrate solution was added and boiled for further 10 min. The heat source was removed, and the solution was stirred for 15 min at room temperature before further cooling down without stirring. For all experiments, ultrapure water (18 MΩ) and phosphate-buffered saline (PBS; Biochrom AG, Berlin, Germany) were used.

The SERS enhancement factor of the gold nanoparticles was estimated by the use of 10^{-6} M crystal violet as described in [33]. Extinction spectra of gold nanoparticles were recorded with a V-670 double-beam ultraviolet–visible (UV–vis)/near-infrared (NIR) spectrophotometer (JASCO, Gross-Umstadt, Germany) showing a plasmon band with maximum at 518 nm (Electronic Supplementary Material (ESM) Fig. S1/S2). UV–vis experiments show that gold nanoparticles are stable in presence of crystal violet in concentrations $<10^{-5}$ M (see ESM Fig. S3). The particle size was determined by

transmission electron microscopy using a Tecnai G2 20S-TWIN microscope (FEI, Hillsboro, USA) to be 14±3 nm (determined as average of 284 nanoparticles).

Cell culture

Swiss albino mouse fibroblast cells (cell line 3T3; DSMZ, Braunschweig, Germany) were maintained in Dulbecco's modified eagle medium (DMEM) supplemented with 10 % fetal calf serum (FCS) and 1 % ZellShield (Biochrom AG, Berlin, Germany) and grown in a humidified environment at 37 °C and 5 % CO_2. Fibroblast cells are characterized by a branched, elongated cell morphology with an average size of 50 μm. For LA-ICP-MS and SERS experiments, 3T3 cells were grown as monolayer on sterile cover-slips (Thermo Fisher Scientific, Waltham, USA) in a six-well plate and incubated with 1 mL of 1 nM gold nanoparticle suspension in standard cell culture medium in a pulse-chase regime. First, fibroblast cells were exposed to 1 nM gold nanoparticles in standard cell culture medium for 30 min ('pulse'). Secondly, the particle suspension was removed, and cell culture medium without nanoparticles was added for varying chase times ranging from 15 min to 48 h. For cell experiments utilizing continuous nanoparticle incubation, fibroblasts were incubated gold nanoparticles for 3 and 24 h.

After nanoparticle exposure, 3T3 cells were washed thoroughly with PBS, immediately fixed with 4 % para-formaldehyde in PBS, and dehydrated in a graded series of ethanol for LA-ICP-MS analysis. For cell synchronization, fibroblast cells were cooled at 4 °C for 1 h [34].

Laser ablation ICP-MS of cells

LA-ICP-MS measurements of fixed fibroblast cells were conducted using an NWR213 laser ablation system (ESI, Fremont, CA, USA) equipped with a two-volume cell was coupled to an ICP sector field mass spectrometer (Element XR, Thermo Fisher Scientific, Bremen, Germany). Details on operating parameters are given in ESM Table S1 and Table S2 of the Supporting Information. The ICP-MS was synchronized with the LA unit in external triggering mode. Helium was used as carrier gas, and argon was added before reaching the ICP torch using a Y-piece. The ICP-MS was tuned daily for maximum ion intensity and good signal stability (relative standard deviation<5 %), keeping the oxide ratio (ThO/Th) below 1 % during ablation of a microscopic glass slide. An average day-to-day coefficient of variation of 12 % for the ^{137}Ba intensity was observed along the analyses. Representative areas of the cell sample with groups of individual fibroblast cells were ablated by continuous line scanning. The laser ablation parameters were optimized for high sensitivity at high spatial resolution and complete cell ablation as described in detail by Drescher et al. [31]. The scan mode is based on the overlap of single ablation points as illustrated in ESM Fig. S4, which is achieved by a repetition rate high enough relative to scan speed. The measured signal reflects the difference in ablated area giving a spot size in scan direction (1.5 μm) smaller than the laser focus point diameter (8 μm). Since a line distance of 7 μm was applied in all LA-ICP-MS experiments, the resulting pixel size is 1.5×7 μm with an area of 10.5 μm^2.

The time-dependent ICP-MS intensities were exported to Origin 9.0 (Originlab Corporations, Northhampton, USA) to convert each raw data point to a single pixel in a color-coded surface plot. The time scale was transformed to a micrometer scale using the selected scan rate of 8 μm s^{-1}. To determine the integrated ^{197}Au$^+$ intensity per single fibroblast cell, the two-dimensional LA-ICP-MS intensity maps were used. ImageJ software was applied to integrate the ^{197}Au$^+$ intensity of each single cell. The integrated intensity of 10-25 fibroblast cells is averaged and given as mean value for each pulse-chase experiment.

ICP-MS analysis of nanoparticle/cell digestion

Fibroblast cells were grown in 75-cm^2 cell culture flasks under standard cell culture conditions as described above. The culture medium was replaced by 10 mL of gold nanoparticle suspension (1 nM) in DMEM with 10 % FCS and 1 % ZellShield. After nanoparticle exposure for different time periods (30 min, 3, and 24 h), cells were washed thoroughly with phosphate-buffered saline (PBS), removed from the cell culture flask by trypsination, washed with 5 mL culture medium and counted. Cell pellets containing 1×10^6 fibroblasts were obtained by centrifugation of the cell suspension and dried at room temperature.

Dried pellets of nanoparticle-incubated fibroblast cells were digested with aqua regia (450 μL hydrochloric acid and 150 μL nitric acid, purified by sub-boiling) for 1 h and sonicated at 80 °C for 2 h. The cell digests were prepared for ICP-MS analysis by appropriate dilution with deionized water (18 MΩ cm, Milli-Q system from Millipore, Eschborn, Germany). For the determination of the Au concentration, an iCAP Qc ICP-MS (Thermo Fisher Scientific, Bremen, Germany) was used. Blanks without and with cells (without gold nanoparticles) were prepared after the same procedure. The operating parameters are given in ESM Table S3. The iCAP Qc was tuned for maximum sensitivity, keeping the oxide ratio (CeO/Ce) below 3 % during nebulization of a multielement tune solution. For the calibration by standard addition, the samples were spiked at different concentration levels with a gold solution prepared by dilution of gold plasma standard Specpure (Alfa Aesar, Karlsruhe, Germany). Lu (ICP standard CertiPUR, Merck, Darmstadt, Germany) was used as internal standard. The calculation of the number of gold nanoparticles per cell was performed according to [25] using

the average nanoparticle diameter of 14 nm determined by TEM.

SERS experiments with fibroblast cells

SERS spectra of fibroblast cells exposed to gold nanoparticles were obtained with a LabRam HR microspectroscopic setup (Horiba Jobin-Yvon GmbH, Bensheim, Germany) equipped with a liquid nitrogen-cooled charge-coupled device detector. All measurements were conducted using a 60× water immersion objective (laser spot size of 1.5 μm), an excitation wavelength of 785 nm (2×10^5 W cm^{-2}) and an acquisition time of 1 s. SERS spectra were recorded between 300 and 1,800 cm^{-1} at a resolution of ~2 cm^{-1}.

Transmission electron microscopy

For transmission electron microscopy (TEM) fibroblast cells were treated with 1 nM Au nanoparticles for 30 min (pulse) and maintained in DMEM supplemented with 10 % FCS for 3 h (chase). The cells were washed thrice with PBS and fixed with 2.5 % glutaraldehyde (SERVA, Heidelberg, Germany) in 0.1 M sodium cacodylate buffer (SERVA, Heidelberg, Germany) for 1 h at room temperature and 20 h at 7 °C. The cells were postfixed with a solution containing 1 % osmium tetroxide and 0.8 % potassium ferrocyanide II in 0.1 M cacodylate buffer for 1.5 h, dehydrated in a graded series of ethanol and transferred to Epon resin (Roth, Karlsruhe, Germany). Ultrathin sections of the cells (70 nm) were stained with uranyl acetate, and lead citrate and were examined with a Zeiss EM 906 electron microscope at 80 kV acceleration voltage (Carl Zeiss SMT GmbH, Oberkochen, Germany).

The size distribution of nanoparticles inside the cells is 14± 4 nm (determined by TEM), which is in accord with the particle size in aqueous suspension. We conclude that the intracellular effects are indeed characteristic of an uptake of nanoparticles of this size.

Results and discussion

Following gold nanoparticle aggregation in single cells using LA-ICP-MS micromapping

To understand the uptake and processing of nanoparticles in living cells, experiments with chase times ranging from 15 min to 48 h were conducted on synchronized 3T3 fibroblast cells after incubation with gold nanoparticles of 14 nm (see ESM Fig. S1 for electron micrograph) in a 30-min pulse. For the localization and quantification of gold nanoparticles inside individual cells by elemental micromapping, we utilized high spatial resolution laser ablation in combination with ICP-MS. Here, the spatially confined laser ablation of the formaldehyde-fixed cells allows to monitor the quantitative distribution of the gold nanoparticles and can provide information on their processing at different time points after the incubation pulse (Fig. 1).

The ^{197}Au$^+$ intensity was determined by continuous ablation line-by-line of an area comprising 10-25 cells for each chase time and plotted as a function of ablation position (for illustration of the laser ablation scan mode see ESM Fig. S4). Figure 1 displays an overlay of the color-encoded ^{197}Au$^+$ local intensity map with the corresponding bright field micrograph of the fibroblast cells. The intensity of the ^{197}Au$^+$ signal scales with the local number of gold nanoparticles [31] and thus gives information about the particle intracellular distribution. The signal obtained from each ablated spot is related to the density and aggregation of the nanoparticles in the endolysosomal vesicles and their accumulation in distinct areas inside the cell. As the variations in the 2D intensity maps indicate, the gold nanoparticles form aggregates of different sizes and the distribution and intensity of ^{197}Au can be compared for the different chase times.

After chase times of 15 min to 1 h (Fig. 1a, b), the ^{197}Au$^+$ signal is homogeneously distributed inside the cells, suggesting the uptake of nanoparticles building small aggregates of a few particles inside the cell or direct uptake of very small aggregates, in accord with previous observations[31] and supported by UV–vis spectra of the gold nanoparticles under cell culture conditions (ESM Fig. S1). Note that detection of a single 14-nm-sized gold nanoparticle is not possible due to the low number of atoms (~85,000) resulting in a low signal/noise ratio. In the next time interval from 1 to 3 h (Fig. 1b–d), a significant increase in high-intensity spots in the perinuclear regions of each cell can be observed. At the same time, the distance between single spots of high intensity is diminished, compared to short chase times. This can be explained by particle accumulation in the proximity of the cell nucleus for times starting from ~3 h, so that each ablated spot in a perinuclear region yields a high ^{197}Au$^+$ signal. Since the cells all contain the same amount of nanoparticles on average (as evidenced from the integrated intensities per cell, gray bars in Fig. 3) due to equal time available for their uptake (equal pulse duration of 30 min for all chase times), the observed changes of the signal intensity and spot density must be attributed to cellular processes that lead to accumulation. The processing of the nanoparticles over time by the cell includes e.g., multivesicular fusion of particle-containing endosomes or particle aggregation inside the vesicles due to changes of the microenvironment, such as decrease in pH value [35, 36].

From 3 to 7 h, the LA-ICP-MS intensity maps in Fig. 1d–g reveal a similar distribution of the ^{197}Au$^+$ signal within the cells, showing many spots of high intensity near the cell nucleus. This situation is also comparable to the distribution of the ^{197}Au$^+$ signal generated by silica-covered gold nanoparticles reported recently [10]. From these observations, we
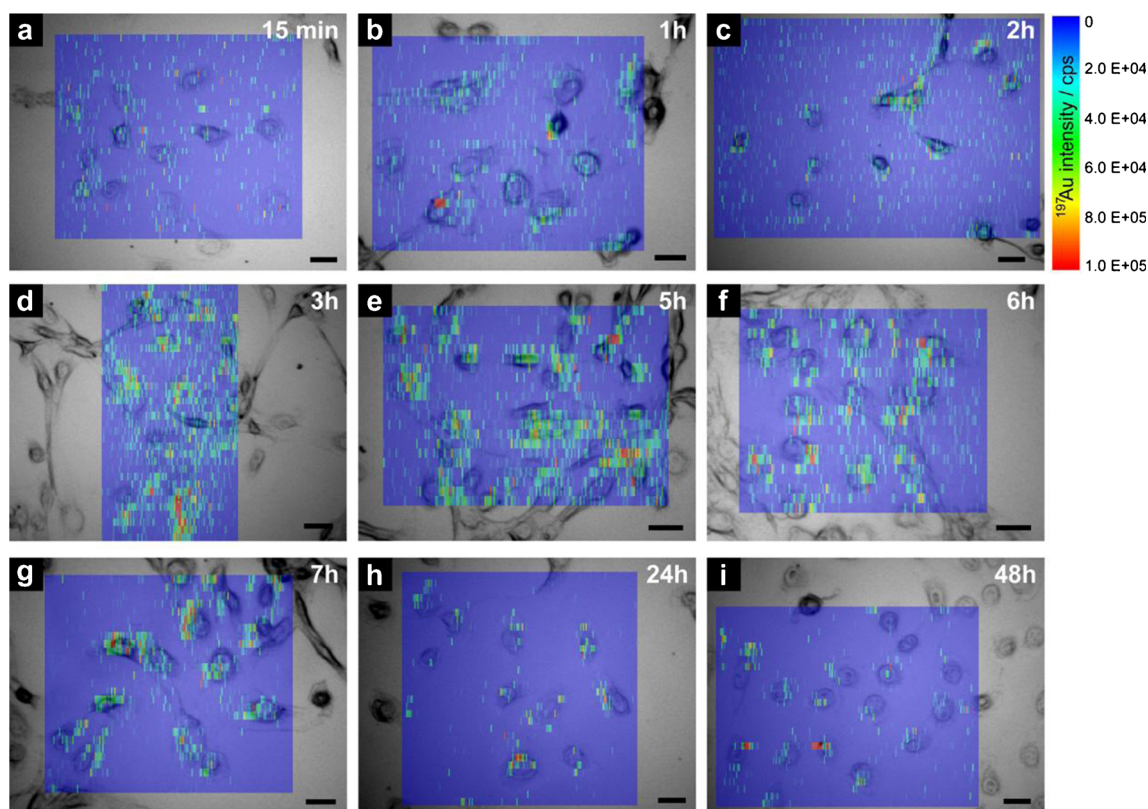
Fig. 1 Bright-field micrographs of fixed 3T3 fibroblast cells superimposed with the corresponding laser ablation ICP-MS images of ^{197}Au$^+$ intensity distribution. Synchronized cells were exposed to 1 nM gold nanoparticles in a pulse-chase regime: an incubation pulse of 30 min and chase times ranging from 15 min to 48 h were applied. For each experiment, 10–25 individual fibroblasts, comprising 150–300 ablation spots per cell, were measured. *Scale bars* represent 25 μm. Parameters: laser spot size, 8 μm; scan speed, 8 μm/s; repetition rate, 5 Hz; pixel size, 1.5×7 μm; fluence, 0.4 J cm^{-2}

infer that, using LA-ICP-MS micromapping, the cellular processes leading to nanoparticle aggregation can be followed and proceed in the time period of 15 min to 3 h. This is also in accord with the time frames envisioned for entry into the late endosomal maturation stage already after relatively short chase times [37, 38]. Similar results regarding intracellular particle accumulation with increasing chase time are obtained in experiments utilizing a different particle concentration for incubation (0.1 nM instead of 1 nM) and for nonsynchronized cells (data are not shown). These experiments illustrate that our LA-ICP-MS results show a high reproducibility also for different exposure parameters.

When chase times are further increased to 24 and 48 h (Fig. 1h, i), the number of high-intensity spots decreases because of particle loss in the course of exocytosis [39, 40] and cell division [41, 42, 18, 43]. The particle aggregates close to the cell nucleus discussed above (see Fig. 1d–g) are still present after 24 and 48 h (Fig. 1h, i). In ESM Fig. S5A, line scans from maps shown in Fig. 1 are displayed; they also illustrate the evolution of signal distribution over time. In conclusion, LA-ICP-MS micromapping indicates proceeding aggregation of nanoparticles with increasing chase time, which is in accord with our previous investigations by electron

microscopy using 30 nm gold nanoparticles in cells at different time points [13]. From the LA-ICP-MS data, it is possible to draw conclusions on the accumulation of nanoaggregates in distinct cellular regions, but not on the number of gold nanoparticles per vesicle and the aggregate geometry and interparticle spacing, the latter having implications for SERS enhancement. Figure 2 displays TEM micrographs of the fixed fibroblast cells after a chase time of 3 h. As expected, gold nanoparticles were found in endosomal vesicles, neither free in the cytoplasm (Fig. 2a) nor in the nucleus (Fig. 2b). Apart from small aggregates, many isolated particles were observed (Fig. 2b, c) in multivesicular structures that are formed during endosomal maturation. The size distribution of gold nanoparticles inside the cells (14±4 nm) is equal to that in suspension (14±3 nm), suggesting that the intracellular processing is characteristic of gold nanoparticles of this size. The localization to intravesicular accumulations is in agreement with the LA-ICP-MS data, where increase in the local ^{197}Au$^+$ signal intensity is observed after a chase time of 3 h (compare Fig. 1d).

Based on the 2D LA-ICP-MS maps of Fig. 1, the relative integrated ^{197}Au$^+$ intensity per single fibroblast cell was determined as mean value of 10-25 cells (Fig. 3, gray bars). The
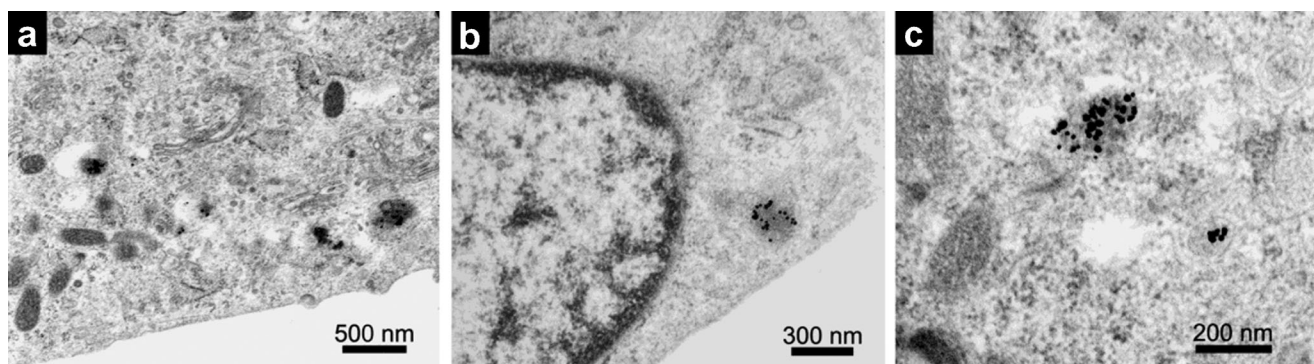
Fig. 2 Transmission electron micrographs of ultrathin sections of 3T3 fibroblast cells incubated with gold nanoparticles (1 nM) in DMEM supplemented with 10 % FCS for 30 min (pulse) and 3 h without gold nanoparticles (chase)

standard deviations are indicative of a relatively high cell-to-cell variability regarding the number of internalized particles, taking also into account differences in cell size and morphology. We also determined the number of spots per cell with $^{197}Au^+$ intensity>50,000 cps as an indicator for the aggregation of nanoparticles inside the fibroblast cells over time (Fig. 3, black bars; see also ESM Fig. S6 for other threshold values). From the relative integrated intensities, we can infer that the number of nanoparticles per single cell is similar within the first 7 h (Fig. 3, gray bars). As expected, the integrated intensities for these chase times (15 min to 7 h) are constant with values >90 % of the highest value in this series (Fig. 3). This is in accord with the fact that each cell has taken up a similar amount of nanoparticles during the 30-min gold nanoparticle pulse (see gray bars in Fig. 3) and that sensitivity of detection is largely independent of aggregation for the nanoparticle/nanoaggregate size range and spot size used in our experiment. The significant decrease in the relative integrated intensity after 24 and 48 h of cultivation in absence

of nanoparticles (Fig. 3) can be attributed to the partitioning of nanoparticles to daughter cells during mitosis[42].

In comparison to the relative integrated intensity, the number of spots with $^{197}Au^+$ intensity>50,000 cps (Fig. 3, black bars) shows a different trend that is attributed to a change in the intracellular particle distribution over time. The lowest values are obtained at the beginning of the chase time period, when only separated nanoparticles and very small aggregates are present. From 15 min to 3 h, an increasing number of high-intensity values per single fibroblast cell are found. This indicates clearly that particle aggregates and likely also accumulations of many aggregate containing endosomes per sampled spot are formed, while the absolute number of nanoparticles per cell stays constant. Thenceforward, the number of high-intensity spots decreases again, with redistribution of the aggregate containing endosomes, yielding fewer aggregates per ablated spot, and subsequent partitioning upon cell division for the very long chase times (black bars in Fig. 3). A similar trend can also be observed for the lower threshold
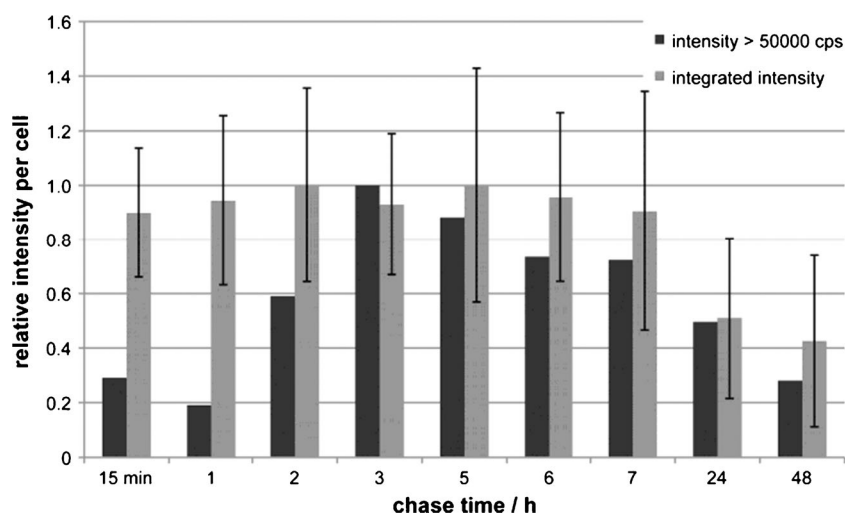
Fig. 3 Relative integrated $^{197}Au^+$ intensity (*gray bars*) and the relative number of spots with an intensity>50,000 cps (*black bars*) of single 3T3 fibroblast cells based on LA-ICP-MS data (see data sets in Fig. 1). The relative integrated intensity is given as mean value of 10-25 fibroblast cells for each chase time. The values are normalized to the maximum. The standard deviation reflects the cell-to-cell variability. The $^{197}Au^+$ intensity of 50,000 cps approximates 1,500 gold nanoparticles of 14 nm in size (see also Figure S6 for the analysis using other threshold values)

value of $^{197}Au^+$ intensities >25,000 cps (see ESM Fig. S6), reflecting different degrees of particle aggregation within the cells. These data confirm the conclusion drawn from the intensity mapping that essential processes of particle processing inside the cell, e.g., cellular uptake, aggregation inside the endosomes, and vesicular transport to the immediate vicinity of the cell nucleus, occur within the first 3 h after uptake.

In order to verify that the $^{197}Au^+$ signal can be used for quantification independent of nanoparticle processing, we also performed LA-ICP-MS micromapping and line scans (ESM Fig. S5B) with cells containing gold nanoparticles in different concentration. To achieve this, fibroblast cells after continuous incubation with 0.1 nM Au nanoparticles for 3 and 24 h were studied. Figure S5B in the ESM shows an increase in the $^{197}Au^+$ signal intensity, indicating a higher gold nanoparticle concentration in the cells due to the longer exposure time.

Furthermore, we determined the average gold nanoparticle amount by lysis of 10^6 fibroblast cells and measurement of their liquid extract by ICP-MS. For the synchronized cells in our 30-min pulse-chase experiments, the number of nanoparticles was determined to 22,000 per cell. It is in good agreement with our previous studies using 30-nm-sized gold nanoparticles [31].

Intracellular particle processing as evidenced by SERS data

In parallel to the LA-ICP-MS experiments, samples of the synchronized fibroblast cells were investigated in Raman mapping experiments as live cells in buffer solution with the same pulse-chase regime. The SERS spectra of living cells are expected to yield qualitative information concerning the composition of the immediate nanoparticle environment, that is, the components from the cell culture medium and the intracellular components adsorbed to the nanoparticle surface, forming a corona [9, 13]. As observed previously for other gold nanoparticles in an epithelial cell line, the SERS

enhancement required for the detection of low concentration biomolecular compounds is related to the formation of nanoparticle aggregates inside the cell, and the spectral fingerprint, as well as the number of bands and the average intensities at signal maxima, can vary greatly with chase time [13]. From the fact that already one nanoparticle aggregate in one probed volume of a spot in a cell (~50 fL) would be sufficient to generate a high SERS signal [44] and assuming that at least one such nanoaggregate must be present in case a SERS spectrum is observed for a sampled spot, the number of SERS spectra per cell can serve as an indicator of the amount of those nanoaggregates that act as SERS substrates. Figure 4 displays the relative number of SERS spectra (normalized to the maximum) obtained per cell after different chase times. Per chase time, >1,000 spectra were screened for SERS signals. The small percentage of SERS spectra in a mapping data set from a cell (4 % at best) is much lower than for other gold nanoparticles administered at similar nanoparticle concentration [9]. This suggests that the amount of nanoparticle aggregates providing sufficient enhancement must be small.

In order to find out whether the amount of SERS-active aggregates may be determined by the number of nanoparticles, and assuming a higher nanoparticle concentration in the cells with longer exposure time (ESM Fig. S5B), we also conducted experiments with the cells exposing them to the nanoparticles for longer times continuously. Interestingly, the number of SERS spectra obtained after 3 and 24 h of such continuous incubation is very similar (see asterisk labels in Fig. 4 for comparison). This indicates that the SERS enhancement is not only related to the amount of nanoparticles (with a higher amount probably resulting in more nanoaggregates), but mainly to aggregate geometry, e.g., interparticle spacing. The SERS enhancement by the nanoaggregates must be determined mainly by the processing of the endocytosed nanoparticles with respect to the cellular ultrastructure.

Furthermore, experiments with the nanoparticles in the absence of cells yielded an enhancement on the order of

Fig. 4 Number of SERS spectra (black bars) and number of spectra containing at least six bands (gray bars). The values are normalized to the maximum number of spectra with a SERS signal (of all experiments). The light gray bars labeled with an asterisk represent the numbers obtained in experiments with continuous nanoparticle exposure (3 and 24 h) for comparison
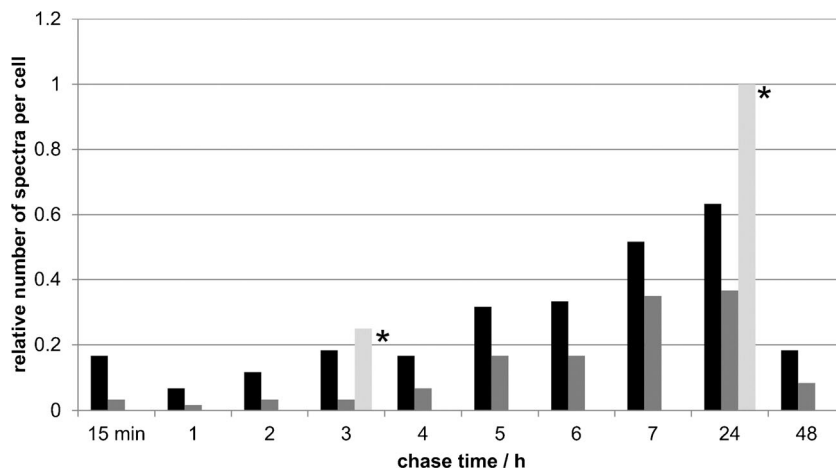
~10^3, in agreement with former studies of nonaggregated 15-nm-sized, citrate-stabilized gold nanoparticles [33]. The addition of sodium chloride, phosphate buffer (ESM Fig. S1) or non-biological analyte molecules such as crystal violet dye (ESM Fig. S3) led to an agglomeration of the nanoparticles as indicated by the absorbance spectra (ESM Fig. S1 and Fig. S3), and to an increase in the enhancement factor to about 10^5, several orders of magnitude smaller than found for other gold nanoaggregates [45].

The number of spectra per cell increases steadily with increasing chase time up to 24 h after the 30-min gold pulse (Fig. 4, black bars). This is in accord with the formation of SERS active aggregates during endosomal maturation, multivesicular fusion, and effects on nanoparticle stability due to the harsh environment in the late endosome/lysosome [14, 15, 46, 47]. After 48 h, the decrease in the number of SERS spectra, similar to the observations made in the case of the samples studied by LA-ICP-MS (Fig, 3), can be explained by a further redistribution of nanoparticles due to cell division and by exocytosis of nanoparticles [18, 40, 43]. Interestingly, after a chase time of 15 min, the number of spectra with SERS signals is slightly higher than at the subsequent two time points (Fig. 4). This signal is likely to be generated due to nanoparticles interacting with the cell membrane without taking part in endocytosis. They take longer than 15 min to detach from the cell membrane and diffuse into the cell culture medium with increasing chase time. A similar observation is made with LA-ICP-MS in the case of the $^{197}Au^+$ high-intensity spots (Fig. 3). These findings are also supported by TEM imaging, suggesting that indeed nanoparticles are in contact with the cell membrane without actually being taken up [13].

The SERS spectra provide information about the molecular composition of the immediate proximity of the gold nanoaggregates at different chase times. As can be deduced from the qualitative changes in the spectral fingerprints, the composition of the endosomal surroundings and the interaction of the nanoaggregates with the biomolecules vary with chase time. Moreover, the SERS enhancement of the nanoaggregates changes. Due to the strong localization of the field and the high field gradients, often only a few bands from a biomolecule are visible in the spectrum. Therefore, the number of bands in a SERS spectrum from a femtoliter-sized volume that is probed in the cell is expected to increase when there are more nanoaggregates with more regions of high local fields present. This observation was made in a SERS study with other nanoparticles and a correlation with nanoaggregate morphologies in a different cell line [13]. As an example, the amount of SERS spectra that contain at least six signals increases with chase time, following the increase in the number of spectra as such (Fig. 4, gray bars), but equaling more than half of the total number of SERS spectra only after ~7 h. At earlier times, the SERS signatures contain fewer bands.

In general, the composition of the biomolecular corona of gold nanoparticles has been found previously to undergo several changes [9, 13, 48]. Figure 5, displaying representative spectra for each time point for the nanoparticles used here, illustrates the influences of the chase time on the SERS spectral fingerprints. With increasing chase time, SERS spectral fingerprints become more homogeneous, repeatedly showing similar signals. Details about the type and frequency of the occurrence of these bands are provided in ESM Table S4.

The spectra at all time points are dominated by bands that can be assigned to vibrational modes of protein side chains. The variation of their frequency of occurrence (details also in ESM Table S4) can be explained by the varying protein–gold nanoaggregates interaction due to the endosomal maturation process, e.g., the decreasing pH inducing structural changes and modification by enzymes [49]. For example, the signals around 500 and 654 cm^{-1}, which can be assigned to the disulfide bond vibration and a C–S vibration of cysteine [50, 51], respectively, are found very frequently after 3 h chase time, while signals around 770 cm^{-1} assigned to the indol breathing vibration of tryptophan side chains [52, 53], COOH deformation in cysteine, leucine or phenylalanine [54], and tyrosine vibrations at 1,138 cm^{-1} and or at 855 cm^{-1} [55], respectively, can be observed more frequently after 5 h chase time (Fig. 5). A further example for structural changes of the interacting proteins due to changes in the endosomal microenvironment is the occurrence of other protein signals at later chase times. Some vibrations assigned to rocking vibration of NH_2 groups or C–N stretching vibrations ~1,070 cm^{-1} and NH_3^+ deformation vibrations at 1,580 cm^{-1} can only be observed at chase times longer than 4 and 2 h, respectively (ESM Table S4). The omnipresence of some spectral patterns, e.g., a band of an S–S stretching vibration around 460 cm^{-1} [50, 54] indicates that some components of the protein corona are adsorbed strongly to the gold nanoparticles throughout the time course of endosomal maturation. So far, most SERS studies on the biomolecule corona of gold nanoparticles that have been conducted with larger nanoparticles have indicated signals from nucleotides, proteins, and lipids [13, 17, 56, 57]. As the spectra obtained with the smaller nanoparticles here reveal, the nano-bio interaction in the case of 14-nm-sized gold nanoparticles is dominated by the contact of the proteins with the gold surface through their side chains. The processing of nanoparticles in a cell is not random, but determined by the physicochemical properties, which differ for different types of nanomaterials, e.g., for nanoparticles of different size [39, 58, 59]. The pulse-chase experiments conducted here will also help to understand the many different signals appearing in experiments reported upon continuous nanoparticle incubation, which usually yield endosomal vesicles from many different maturation stages at the same time [12].
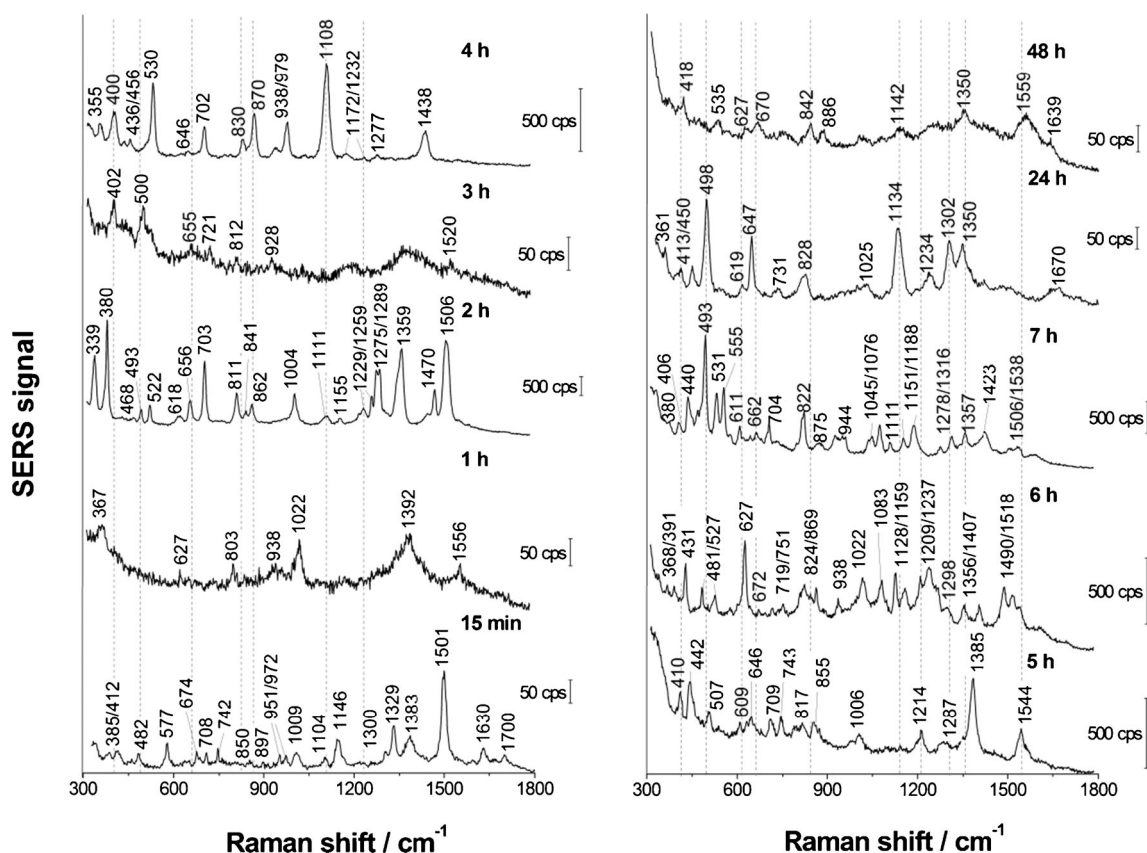
Fig. 5 SERS spectra (representative examples extracted from mapping data sets) obtained from synchronized 3T3 fibroblast cells after 30 min exposure to gold nanoparticles followed by different chase times (15 min to 48 h) in cell culture medium in absence of nanoparticles. Excitation wavelength, 785 nm; excitation intensity, $1.9°10^5$ W/cm^2; acquisition time, 1 s

Relating SERS data to nanoparticle/nanoaggregate quantification

The combination of the LA-ICP-MS results and the SERS spectra recorded at the same experimental conditions provides a consolidated view on the nanoparticle localization, distribution, and nanoaggregate accumulation over time, as well as on molecular changes caused by endosomal maturation. The central aim of this work is to find out whether the SERS spectra can be related to the processing of the nanoparticles by the cell using LA-ICP-MS micromapping as indicator of the gold nanoparticle amount and aggregation. From experiments outside cells and theoretical considerations, it is well-known that the geometry of the nanoparticle aggregates that are formed is a crucial determinant of the SERS enhancement factors [60, 61]. Significantly increased fields in nanoparticle dimers and multimers rather than individual nanoparticles give rise to the SERS spectra obtained in vivo [13]. From the great difference in the enhancement factors of nanoaggregates and those of individual gold nanoparticles of the same size range [33] and our knowledge from ultrastructure investigations [9, 13], we conclude that those sampling volumes yielding high

intensity SERS spectra (Fig. 5) must contain one or more nanoparticle aggregates rather than individual nanoparticles.

Even though the integrated intensity of the ^{197}Au$^+$ signal in the LA-ICP-MS experiment is independent of the chase time due to identical length of the gold incubation pulse in all samples (Fig. 3), the presence of nanoaggregates in the cell leads *locally* to high intensities in ^{197}Au$^+$ detection, as evidenced by the distribution (Fig. 1) and number (Fig. 3) of spots with a threshold signal of >50,000 cps. The 2D LA-ICP-MS maps (Fig. 1) reveal the accumulation of the gold nanoaggregates (Fig. 3) in the proximity to the cell nucleus with increasing chase times. Molecular information from these regions can be obtained by SERS (Fig. 5) with an increase in the number of spectra per cell (Fig. 4).

Assuming aggregation of the nanoparticles and accumulation of nanoaggregate containing endosomes to exert an influence on both the SERS and the LA-ICP-MS data, we compare the number of spots per cell yielding a SERS signal with those that display an intensity >50,000 cps in the LA-ICP-MS mapping in Fig. 6 for the different chase times. It should be noted that the LA-ICP-MS data provide information about the amount of gold, independently of the number of individual nanoaggregates, and the amount of SERS spectra is

also independent of the number of "quantized" nanoaggregates in a focal volume. Even though the lateral resolution in both experiments differs only slightly, we refrain from normalization to probed area due to completely different sampling mechanisms. However, compared to the size of nanoparticles, nanoaggregates, and even relatively large endosomal structures, both spot sizes (1.8 μm² for SERS and 10.5 μm² for LA-ICP-MS) are on the same order of magnitude. In the following, we mainly discuss the development of the spectra/high-intensity spot numbers in the course of the chase time, and the absolute numbers provided in Fig. 6 for both methods are not to scale.

The evolution of the total numbers of spectra and high-intensity $^{197}Au^+$ spots per single fibroblast cell (Fig. 6) display different trends, with the number of SERS spectra lagging behind the increase in high-intensity $^{197}Au^+$ spots. While the local gold concentration apparently increases with longer chase times, as indicated by the number of intense spots in the LA-ICP-MS maps, reaching a maximum after 3 h, the number of SERS spectra obtained under the same incubation conditions rises more slowly. It increases gradually and has a maximum after 24 h, at a time when all gold nanoparticles must be contained in late endosomes and lysosomes [42, 62]. This behavior can be interpreted by different SERS enhancement factors, which strongly depend on aggregate morphology and the interparticle distance. The observation that the local gold concentration rises faster than the SERS signals suggests that the many gold nanoparticles in an ablated spot are not necessarily contained in an aggregate with properties that enable high SERS enhancement. Provided that a nanoaggregate possesses a geometry and interparticle spacing that supports SERS enhancement, typically very few "hot spots" in such an aggregate can be responsible for the signal [63, 64]. Specifically at earlier time points, it is possible that LA-ICP-MS probes multiple vesicles with individual

nanoparticles or multivesicular inclusions, which may not provide suitable interparticle spacing for SERS. In good agreement with this conclusion, such structures have been observed in the TEM data for the 3 h chase time (Fig. 2), also in accord with observations of gold nanoparticles of slightly greater size in cells by combined SERS and TEM [13].

From 3 h onward, the number of LA-ICP-MS high-intensity spots decreases again (Fig. 6, blue bars). This decrease reflects a concentration of the gold nanoparticles in fewer and fewer spots, each of which displays even higher $^{197}Au^+$ intensity, so that a constant integrated intensity is maintained (Fig. 3, gray bars). This is also supported by the data displayed in the maps of Fig. 1e–g. In agreement with the localized perinuclear accumulation of the gold nanoparticles, in late endosomes and lysosomes, more aggregates are formed that provide high SERS enhancement, as is reflected by the rising number of SERS spectra. After mitosis (Fig. 6, 48 h chase time), the nanoparticle containing vesicles are divided up between the daughter cells, and the physiological situation may lead to reorganization of the endosomal system, e.g., when the daughter cell starts to reuse lysosomes [41, 42].

Conclusions

We have discussed here the combination of SERS spectra with information on gold nanoparticle and nanoaggregate amount obtained by LA-ICP-MS micromapping during the endosomal maturation process following a 30-min nanoparticle incubation pulse. The results have relevance regarding two aspects: (i) the possibility to relate nanomaterial uptake, localization, and processing information to molecular composition of the nanoparticle corona and (ii) the ability of assessing the efficiency of gold nanoaggregates as SERS nanoprobes by

Fig. 6 Comparison of the number of SERS spectra and the number of high-intensity spots (>50,000 cps) determined by LA-ICP-MS per single fibroblast cell. The number of SERS spectra and high LA-ICP-MS intensity spots are given as mean values of 5 and 10-25 fibroblast cells, respectively. The absolute numbers for both methods are not to scale
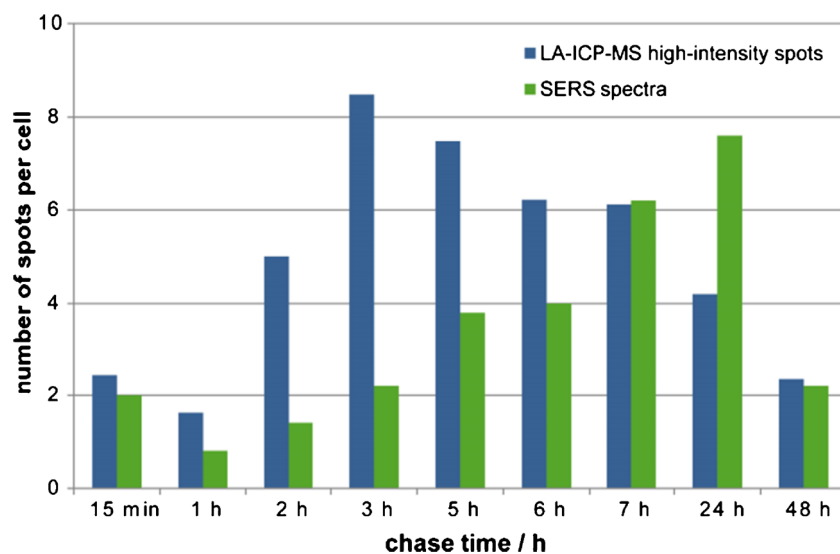
combining information about the SERS characteristics with spatially resolved nanoaggregate quantification. The SERS spectra indicate that mainly proteins interact with the gold nanoparticle surface and that interaction with some functional groups persists throughout the endosomal maturation process. As evidenced by the analysis of LA-ICP-MS data, during processing, the nanoaggregates accumulate in localized, perinuclear regions of the cells, and reorganization occurs during mitosis.

As indicated by relatively small numbers of SERS spectra in spite of many positions with high local gold nanoparticle concentration for earlier endosomal maturation stage, and more SERS spectra per cell in the later stage, the cellular processing must determine nanoaggregate geometry. Data from TEM provide evidence that, at times when nanoparticle accumulation is evident from the LA-ICP-MS micro-maps, large interparticle distances and multivesicular inclusions can occur and prevent sufficient SERS enhancement from taking place. The results obtained here will help to evaluate different types of plasmonic nanostructures regarding their use as SERS nanoprobes for intracellular applications and nanotoxicity studies.

References

1. Thanh NTK, Rosenzweig Z (2002) Development of an aggregation-based immunoassay for anti-protein A using gold nanoparticles. Anal Chem 74(7):1624–1628
2. Stewart ME, Anderton CR, Thompson LB, Maria J, Gray SK, Rogers JA, Nuzzo RG (2008) Nanostructured plasmonic sensors. Chem Rev 108(2):494–521
3. Aroca RF, Alvarez-Puebla RA, Pieczonka N, Sanchez-Cortez S, Garcia-Ramos JV (2005) Surface-enhanced Raman scattering on colloidal nanostructures. Adv Colloid Interface Sci 116(1–3):45–61
4. Stuart DA, Yuen JM, Lyandres NSO, Yonzon CR, Glucksberg MR, Walsh JT, Van Duyne RP (2006) In vivo glucose measurement by surface-enhanced Raman spectroscopy. Anal Chem 78(20):7211–7215
5. Giljohann DA, Seferos DS, Daniel WL, Massich MD, Patel PC, Mirkin CA (2010) Gold nanoparticles for biology and medicine. Angew Chem Int Ed Engl 49(19):3280–3294
6. Dreaden EC, Alkilany AM, Huang XH, Murphy CJ, El-Sayed MA (2012) The golden age: gold nanoparticles for biomedicine. Chem Soc Rev 41(7):2740–2779
7. Boisselier E, Astruc D (2009) Gold nanoparticles in nanomedicine: preparations, imaging, diagnostics, therapies and toxicity. Chem Soc Rev 38(6):1759–1782
8. Dykman L, Khlebtsov N (2012) Gold nanoparticles in biomedical applications: recent advances and perspectives. Chem Soc Rev 41(6):2256–2282
9. Drescher D, Guttmann P, Büchner T, Werner S, Laube G, Hornemann A, Tarek B, Schneider G, Kneipp J (2013) Specific biomolecule corona is associated with ring-shaped organization of silver nanoparticles in cells. Nanoscale 5(19):9193–9198
10. Drescher D, Zeise I, Traub H, Guttmann P, Seifert S, Büchner T, Jakubowski N, Schneider G, Kneipp J (2014) In situ characterization of SiO$_2$ nanoparticle biointeractions using BrightSilica. Adv Funct Mater. doi:10.1002/adfm.201304126
11. Kang B, Mackey MA, El-Sayed MA (2010) Nuclear targeting of gold nanoparticles in cancer cells induces DNA damage, causing cytokinesis arrest and apoptosis. J Am Chem Soc 132(5):1517–1519
12. Kneipp J, Kneipp H, Wittig B, Kneipp K (2010) Following the dynamics of pH in endosomes of live cells with SERS nanosensors. J Phys Chem C 114(16):7421–7426
13. Kneipp J, Kneipp H, McLaughlin M, Brown D, Kneipp K (2006) In vivo molecular probing of cellular compartments with gold nanoparticles and nanoaggregates. Nano Lett 6(10):2225–2231
14. Wilschut J, Hoekstra D (1984) Membrane fusion: from liposomes to biological membranes. Trends Biochem Sci 9(11):479–483
15. Mellman I, Fuchs R, Helenius A (1986) Acidification of the endocytic and exocytic pathways. Annu Rev Biochem 55(1):663–700
16. Kneipp J, Kneipp H, Wittig B, Kneipp K (2007) One- and two-photon excited optical pH probing for cells using surface-enhanced Raman and hyper-Raman nanosensors. Nano Lett 7(9):2819–2823
17. Ochsenkühn MA, Jess PRT, Stoquert H, Dholakia K, Campbell CJ (2009) Nanoshells for surface-enhanced Raman spectroscopy in eukaryotic cells: cellular response and sensor development. ACS Nano 3(11):3613–3621
18. Drescher D, Kneipp J (2012) Nanomaterials in complex biological systems: insights from Raman spectroscopy. Chem Soc Rev 41(17):5780–5799
19. Aaron J, Travis K, Harrison N, Sokolov K (2009) Dynamic imaging of molecular assemblies in live cells based on nanoparticle plasmon resonance coupling. Nano Lett 9(10):3612–3618
20. Rosman C, Pierrat S, Henkel A, Tarantola M, Schneider D, Sunnick E, Janshoff A, Sönnichsen C (2012) A new approach to assess gold nanoparticle uptake by mammalian cells: combining optical dark-field and transmission electron microscopy. Small 8(23):3683–3690
21. Austin LA, Kang B, Yen C-W, El-Sayed MA (2011) Plasmonic imaging of human oral cancer cell communities during programmed cell death by nuclear-targeting silver nanoparticles. J Am Chem Soc 133(44):17594–17597
22. Li KR, Stockman MI, Bergman DJ (2003) Self-similar chain of metal nanospheres as an efficient nanolens. Phys Rev Lett 91(22):227402
23. Shalaev VM (1996) Electromagnetic properties of small-particle composites. Phys Rep 272(2–3):61–137
24. McMahon J, Henry A-I, Wustholz K, Natan M, Freeman R, Van Duyne R, Schatz G (2009) Gold nanoparticle dimer plasmonics: finite element method calculations of the electromagnetic enhancement to surface-enhanced Raman spectroscopy. Anal Bioanal Chem 394(7):1819–1825
25. Chithrani BD, Ghazani AA, Chan WCW (2006) Determining the size and shape dependence of gold nanoparticle uptake into mammalian cells. Nano Lett 6(4):662–668
26. Alkilany AM, Nagaria PK, Hexel CR, Shaw TJ, Murphy CJ, Wyatt MD (2009) Cellular uptake and cytotoxicity of gold nanorods: molecular origin of cytotoxicity and surface effects. Small 5(6):701–708
27. Becker JS, Zoriy M, Matusch A, Wu B, Salber D, Palm C, Becker JS (2010) Bioimaging of metals by laser ablation inductively coupled plasma mass spectrometry (LA-ICP-MS). Mass Spectrom Rev 29(1):156–175
28. Giesen C, Wäntig L, Mairinger T, Drescher D, Kneipp J, Roos PH, Panne U, Jakubowski N (2011) Iodine as an elemental marker for imaging of single cells and tissue sections by laser ablation

inductively coupled plasma mass spectrometry. J Anal At Spectrom 26(11):2160–2165

29. Konz I, Fernandez B, Fernandez ML, Pereiro R, Gonzalez H, Alvarez L, Coca-Prados M, Sanz-Medel A (2013) Gold internal standard correction for elemental imaging of soft tissue sections by LA-ICP-MS: element distribution in eye microstructures. Anal Bioanal Chem 405(10):3091–3096

30. Niehoff AC, Moosmann A, Sobbing J, Wiehe A, Mulac D, Wehe CA, Reifschneider O, Blaske F, Wagner S, Sperling M, von Briesen H, Langer K, Karst U (2014) A palladium label to monitor nanoparticle-assisted drug delivery of a photosensitizer into tumor spheroids by elemental bioimaging. Metallomics 6(1):77–81

31. Drescher D, Giesen C, Traub H, Panne U, Kneipp J, Jakubowski N (2012) Quantitative imaging of gold and silver nanoparticles in single eukaryotic cells by laser ablation ICP-MS. Anal Chem 84(22):9684–9688

32. Tkachenko A, Xie H, Franzen S, Feldheim DL (2005) Assembly and characterization of biomolecule-gold nanoparticle conjugates and their use in intracellular imaging. In: Rosenthal SJ, Wright DW (eds) Nanobiotechnology protocols, vol 303. Methods in molecular biology. Humana Press, pp 85–99. doi:10.1385/1-59259-901-x:085

33. Joseph V, Matschulat A, Polte J, Rolf S, Emmerling F, Kneipp J (2011) SERS enhancement of gold nanospheres of defined size. J Raman Spectrosc 42(9):1736–1742

34. Lindl T. GG (2008) Zell- und Gewebekultur, vol 6. Spektrum Akademischer Verlag

35. Xu S, Olenyuk BZ, Okamoto CT, Hamm-Alvarez SF (2013) Targeting receptor-mediated endocytotic pathways with nanoparticles: Rationale and advances. Adv Drug Deliver Rev 65(1):121–138

36. Salzman NH, Maxfield FR (1989) Fusion accessibility of endocytic compartments along the recycling and lysosomal endocytic pathways in intact-cells. J Cell Biol 109(5):2097–2104

37. Geisow MJ, Evans WH (1984) pH in the endosome—measurements during pinocytosis and receptor-mediated endocytosis. Exp Cell Res 150(1):36–46

38. Murphy RF, Powers S, Cantor CR (1984) Endosome pH measured in single cells by dual fluorescence flow-cytometry—rapid acidification of insulin to pH-6. J Cell Biol 98(5):1757–1762

39. Chithrani BD, Chan WCW (2007) Elucidating the mechanism of cellular uptake and removal of protein-coated gold nanoparticles of different sizes and shapes. Nano Lett 7(6):1542–1550

40. Sakhtianchi R, Minchin RF, Lee K-B, Alkilany AM, Serpooshan V, Mahmoudi M (2013) Exocytosis of nanoparticles from cells: Role in cellular retention and toxicity. Adv Colloid Interface Sci 201–202: 18–29

41. Imoto Y, Yoshida Y, Yagisawa F, Kuroiwa H, Kuroiwa T (2011) The cell cycle, including the mitotic cycle and organelle division cycles, as revealed by cytological observations. J Electron Microsc 60:S117–S136

42. Yan Y, Lai ZW, Goode RJA, Cui JW, Bacic T, Kamphuis MMJ, Nice EC, Caruso F (2013) Particles on the move: intracellular trafficking and asymmetric mitotic partitioning of nanoporous polymer particles. ACS Nano 7(6):5558–5567

43. Sirimuthu NMS, Syme CD, Cooper JM (2010) Monitoring the uptake and redistribution of metal nanoparticles during cell culture using surface-enhanced Raman scattering spectroscopy. Anal Chem 82(17):7369–7373

44. Kneipp K, Wang Y, Kneipp H, Perelman LT, Itzkan I, Dasari RR, Feld MS (1997) Single molecule detection using surface-enhanced Raman scattering (SERS). Phys Rev Lett 78:1667

45. Kneipp J, Kneipp H, Kneipp K (2008) SERS-a single-molecule and nanoscale tool for bioanalytics. Chem Soc Rev 37(5):1052–1060

46. Khlebtsov N, Dykman L (2011) Biodistribution and toxicity of engineered gold nanoparticles: a review of in vitro and in vivo studies. Chem Soc Rev 40(3):1647–1671

47. Stoorvogel W, Strous GJ, Geuze HJ, Oorschot V, Schwartzt AL (1991) Late endosomes derive from early endosomes by maturation. Cell 65(3):417–427

48. Maiorano G, Sabella S, Sorce B, Brunetti V, Malvindi MA, Cingolani R, Pompa PP (2010) Effects of cell culture media on the dynamic formation of protein–nanoparticle complexes and influence on the cellular response. ACS Nano 4(12):7481–7491

49. Anderson DE, Becktel WJ, Dahlquist FW (1990) pH-Induced denaturation of proteins: a single salt bridge contributes 3–5 kcal/mol to the free energy of folding of T4 lysozyme. Biochemistry 29(9):2403–2408

50. Parker FS (1983) Applications of infrared, Raman, and resonance Raman spectroscopy in biochemistry. Plenum Press, New York and London

51. Diaz Fleming G, Finnerty JJ, Campos-Vallette M, Célis F, Aliaga AE, Fredes C, Koch R (2009) Experimental and theoretical Raman and surface-enhanced Raman scattering study of cysteine. J Raman Spectrosc 40(6):632–638

52. Stewart S, Fredericks PM (1999) Surface-enhanced Raman spectroscopy of amino acids adsorbed on an electrochemically prepared silver surface. Spectrochim Acta Part A Mol Biomol Spectrosc 55(7–8): 1641–1660

53. Kim SK, Kim MS, Suh SW (1987) Surface-enhanced Raman scattering (SERS) of aromatic amino acids and their glycyl dipeptides in silver sol. J Raman Spectrosc 18(3):171–175

54. Podstawka E, Ozaki Y, Proniewicz LM (2005) Part III: Surface-enhanced Raman scattering of amino acids and their homodipeptide monolayers deposited onto colloidal gold surface. Appl Spectrosc 59(12):1516–1526

55. De Gelder J, De Gussem K, Vandenabeele P, Moens L (2007) Reference database of Raman spectra of biological molecules. J Raman Spectrosc 38(9):1133–1147

56. Ando J, Fujita K, Smith NI, Kawata S (2011) Dynamic SERS imaging of cellular transport pathways with endocytosed gold nanoparticles. Nano Lett 11(12):5344–5348

57. Tang H-W, Yang XB, Kirkham J, Smith DA (2007) Probing intrinsic and extrinsic components in single osteosarcoma cells by near-infrared surface-enhanced Raman scattering. Anal Chem 79(10): 3646–3653

58. Brandenberger C, Muhlfeld C, Ali Z, Lenz AG, Schmid O, Parak WJ, Gehr P, Rothen-Rutishauser B (2010) Quantitative evaluation of cellular uptake and trafficking of plain and polyethylene glycol-coated gold nanoparticles. Small 6(15):1669–1678

59. Lundqvist M, Stigler J, Elia G, Lynch I, Cedervall T, Dawson KA (2008) Nanoparticle size and surface properties determine the protein corona with possible implications for biological impacts. Proc Natl Acad Sci U S A 105(38):14265–14270

60. Inoue M, Ohtaka K (1983) Surface enhanced Raman scattering by metal spheres. I Cluster Effect J Phys Soc Jpn 52(11):3853–3864

61. Nordlander P, Oubre C, Prodan E, Li K, Stockman MI (2004) Plasmon hybridization in nanoparticle dimers. Nano Lett 4(5):899–903

62. Huotari J, Helenius A (2011) Endosome maturation. EMBO J 30(17): 3481–3500

63. Kneipp K, Wang Y, Kneipp H, Itzkan I, Dasari RR, Feld MS (1996) Population pumping of excited vibrational states by spontaneous surface-enhanced Raman scattering. Phys Rev Lett 76(14):2444

64. Kneipp K, Kneipp H (2013) Probing the plasmonic near-field by one- and two-photon excited surface enhanced Raman scattering. Beilstein J Nanotechnol 4:834–842